Cross-plan Si/Si Ge superlattice acoustic and thermal properties measurement by picosecond ultrasonics

Y. Ezzahri, S. Grauby, S. Dilhaire, J. M. Rampnoux, and W. Claeys

Citation: Journal of Applied Physics **101**, 013705 (2007); doi: 10.1063/1.2403236
View online: http://dx.doi.org/10.1063/1.2403236
View Table of Contents: http://scitation.aip.org/content/aip/journal/jap/101/1?ver=pdfcov
Published by the AIP Publishing

Cross-plan Si/SiGe superlattice acoustic and thermal properties measurement by picosecond ultrasonics

Y. Ezzahri,[a] S. Grauby, S. Dilhaire, J. M. Rampnoux, and W. Claeys
Centre de Physique Moléculaire Optique et Hertzienne (CPMOH), Université Bordeaux 1, 351 Cours de la Libération, 33405 Talence Cedex, France

(Received 24 February 2006; accepted 19 October 2006; published online 8 January 2007)

A pump-probe thermoreflectance technique is used for the nondestructive evaluation of thermal and acoustic properties of $Si/Si_{0.7}Ge_{0.3}$ superlattice (SL) at room temperature. In particular, this technique allows the determination of the metal transducer/SL thermal boundary resistance, the SL cross-plan thermal conductivity, and the longitudinal sound velocity inside the SL. Several effects related to the extraction of these properties are studied, including the metal transducer thickness and electron diffusion inside it. © *2007 American Institute of Physics*. [DOI: 10.1063/1.2403236]

I. INTRODUCTION

Multilayers and superlattices have become one of the most investigated research areas in semiconductors physics.[1] Since the beginning in the 70's,[2,3] a wide spectrum of experimental and theoretical investigations has been carried out. These structures exhibit spectacular thermal, electrical, and optical properties which do not exist inside any natural crystals. This degree of freedom offered in semiconductor research through advanced materials engineering has brought about ideas for applications. The promise of improved thermoelectric materials and problems of thermal management of microelectronic and optoelectronic devices have stimulated more extensive studies of semiconductor superlattices.

High figures of merit (Z) have recently been reported[4,5] for thermoelectric materials based on Bi_2Te_3/Sb_2Te_3 superlattices and PbSeTe quantum dots superlattices at room temperature. This enhancement might be due to a possible thermal conductivity reduction in low dimensional structures. A variety of semiconductor superlattices has been tested[6–12] and most of the results tally with the fact that these structures are characterized by a thermal conductivity lower than that of corresponding bulk materials or solid solution alloys. Results are highly dependent on the superlattice period and the interface quality.[9,10,13] To explain observations, many models have been proposed based separately on the diffusive regime[14] using Fourier equation, or the ballistic regime[15–17] using Boltzmann transport model.

The most commonly used technique to measure the thermal conductivity of thin semiconductor films is the 3ω method developed by Cahill.[18] Reliable data obtained with this method are now becoming available. A second interesting method is the pump-probe thermoreflectance technique (PPTT). Thermal transport experiments using this technique were reported in Ref. 19. PPTT provides a direct noncontact method for measuring heat transport on nanometer length scales. Most engineering materials exhibit a thermal diffusivity α in the range of $5\times10^{-3}<\alpha<1\ \mathrm{cm^2/s}$, and at $t=200$ ps, heat diffusion lengths $l=\sqrt{\alpha t}$ are in the range of $10<l<140$ nm.[13] Therefore PPTT offers nanometer-scale depth resolution, and more specifically, it can isolate the effect of interface conductance from thermal conductivity of a thin layer.[20] By contrast 3ω method cannot differentiate the thermal conductivity of a film and the thermal conductance of its interfaces.

In this paper, we use PPTT to study phonon transport in different Si/SiGe superlattices at room temperature. First, we start with a description of the samples and of the experimental setup. Second, we present the thermal model describing heat diffusion inside the structure once the pump pulse is absorbed. The model is based on solving Fourier classical heat diffusion equation in Laplace domain by taking into account electron diffusion inside the metal film. In the discussion, we will differentiate thermal contribution from acoustic contribution to the PPTT signal. The thermal contribution is then fitted with a theoretical model in order to determine the thermal properties of the sample.

II. SAMPLES DESCRIPTION AND EXPERIMENTAL SETUP

Results on four samples are presented in this paper. Each one is made of a 1 μm $Si/Si_{0.7}Ge_{0.3}$ superlattice (SL), grown on about 500 μm silicon substrate, and coated by an Al "transducer" film. The term "transducer" is used to specify the role of the metal film: it converts light energy into heat which creates an acoustic wave propagating deeply in the active structure. By this way, the transducer generates the necessary acoustic vector for the analysis of the acoustic contribution in the PPTT signal. Identified thicknesses of the Al film vary from 86 to 474 nm. A 2 μm buffer layer was grown between the SL and the substrate in order to reduce mechanical stress between the substrate and the active SL due to the lattice mismatch between silicon and germanium which is about 4.2%.[21] Figures 1(a) and 1(b) show, respectively, a schematic diagram of the experimental setup and a transmission electron microscopy picture of one of the studied samples. A pulsed laser beam from a 80 MHz Ti:sapphire laser with a pulse duration of 100 fs at $\lambda=780$ nm is separated into two beams with an intensity ratio of 10:1 by a

[a]Present address: Department of Electrical Engineering, University of California, Santa Cruz, California 95064; electronic mail: younes@soe.ucsc.edu

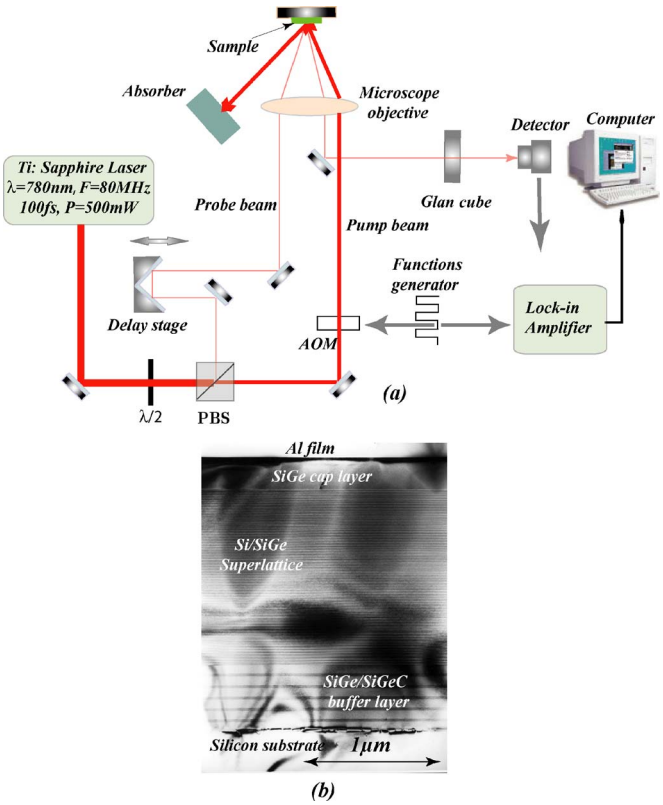

FIG. 1. (Color online) (a) Schematic diagram of the PPTT experimental setup and (b) a transmission electron microscopy picture of one of the studied samples with the different constituting layers.

polarizing beam splitter associated to a zero order $\lambda/2$ plate. The intense "pump" beam is used to heat the metal film, while the weaker "probe" beam is used to monitor the reflectivity variation of its surface, which can be related to its temperature variation. The pump beam passes through an acousto-optic modulator (AOM) that creates a pulse train modulated at a frequency of 574 kHz. The pump beam is focused to $\sim 20\ \mu$m. The probe beam is reflected off a retroreflector mounted on a mechanical translation stage to increase the optical path length of the probe beam as well as the time delay between the pump and the probe pulses. The probe, which is centered in the heated area created by the pump pulse, is focused to $\sim 6\ \mu$m at near normal incidence. A polarizer, oriented in such a way that only the probe beam can cross it, is positioned before the photodiode which monitors the probe beam reflection off the sample. To improve the signal to noise ratio, the detector response at 574 kHz is then monitored by a lock-in amplifier locked on 574 kHz and computer analyzed.

III. HEAT TRANSPORT THEORETICAL MODELING

In a PPTT, determining thermal conductivity and interface thermal resistance is carried out by comparing the experimental cooling curve with the theoretical model and optimizing the free parameters. When the pump light is absorbed, its energy is at first communicated to electrons near the front surface of Al film which are excited to higher energy states. These hot electrons constitute the heat source term and quickly diffuse away from the Al surface at a distance which largely exceeds the optical penetration depth, but still confined in the Al film by the Schottky barrier at the interface Al/SL. To take into account this process, we introduce a new parameter ς, which represents the heat source penetration depth. Within several picoseconds, hot electrons transfer their energy to the lattice by phonon emission or electron-phonon collisions, raising slightly the Al film temperature. Prior works have shown that the time necessary for electron gas energy relaxation into phonon bath was <2 ps for metals.[22–24] After that time, the metal film can be characterized by a macroscopic temperature which is the lattice temperature. To make sure that diffusive regime is well established, we consider the time scale in our model starting from 5 ps. Figure 2 shows a schematic diagram of the studied structure with the spatial coordinate in the cross-plan direction.

The time scale of the experiment is ~ 1 ns. In this case, since the transducer thickness largely exceeds its optical penetration depth ξ, which is $\xi \approx 7$ nm at $\lambda \approx 780$ nm for Al, heat diffusion within the metal film cannot be neglected. To model the heat propagation along the cross-plan direction of the structure after the laser pump pulse is absorbed, we use Fourier classical heat diffusion equation (the flux heat is proportional to the temperature gradient),[25] in which we make four assumptions: (i) penetration of the heat source inside the metal transducer is being taken into account; (ii) due to the short time scale of the experiment, the active subjacent semiconductor layer to the Al metal transducer behaves like a semi-infinite medium; neither the buffer layer nor the substrate will affect the temperature variation of the Al top surface; (iii) if we take into account the short time scale of the experiment, the spot pump diameter ($\sim 20\ \mu$m) is much larger than the explored depth inside the structure, therefore it is legitimate to assume a one-dimensional thermal problem, thus we can disregard radial transport;[9] and (iv) since the time scale of the experiment is extremely short, the heat flux at the free surface of the Al metal transducer is not taken into account. The flow of heat in the whole structure is then governed by the following equations:

$$\beta_f^{\perp}\frac{\partial^2 T_f}{\partial z^2} - (\rho C)_f \frac{\partial T_f}{\partial t} + S(z,t) = 0,$$
$$\beta_s^{\perp}\frac{\partial^2 T_s}{\partial z^2} - (\rho C)_s \frac{\partial T_s}{\partial t} = 0. \tag{1}$$

T_f and T_s are the temperature distributions within the Al metal transducer and the subjacent semiconductor layer, respectively. $(\rho C)_f$ and $(\rho C)_s$ are, respectively, specific heat per unit volume of the Al transducer and the active subjacent semiconductor layer. $\beta_f^{\perp}$ and $\beta_s^{\perp}$ are, respectively, the normal components of their thermal conductivities. $S(z,t)$ represents the heat source term given by

$$S(z,t) = \frac{(1-R)Q}{A\varsigma}\delta(t)\exp\left(-\frac{z}{\varsigma}\right) = S_0\delta(t)\exp\left(-\frac{z}{\varsigma}\right). \tag{2}$$

R is the reflection coefficient of the Al transducer at normal incidence, Q is the pump pulse power, A is the Al surface area illuminated by the pump pulse, and $\delta(t)$ is the Dirac

delta function. Expression (2) represents an exponential decay of the heat source with a characteristic length ς.

Initial and boundary conditions are given by

$$T_f(t=0)=T_s(t=0)=0,$$

$$\frac{\partial T_f}{\partial z}(z=0,t)=0, \tag{3}$$

$$T_s(\infty,t)=0.$$

Continuity of heat flux at the interface Al transducer/active subjacent semiconductor layer and the thermal behavior of this interface are represented by

$$\beta_f^{\perp}\frac{\partial T_f}{\partial z}(z=d_f,t)=\beta_s^{\perp}\frac{\partial T_s}{\partial z}(z=0,t),$$

$$[T_f(z=d_f,t)-T_s(z=0,t)]=-R_K\beta_s^{\perp}\frac{\partial T_s}{\partial z}(z=0,t). \tag{4}$$

As we can see in this formula, we have made a referential change which will not affect the final results. The solution of the equation system (1) becomes simpler in Laplace domain, in which it takes the form

$$\frac{\partial^2\theta_f}{\partial z^2}-q_f^2\theta_f+\chi\exp(-az)=0,$$

$$\frac{\partial^2\theta_s}{\partial z^2}-q_s^2\theta_s=0, \tag{5}$$

where $q_{f,s}^2=p/\alpha_{f,s}^{\perp}$, $\chi=S_0/\beta_f^{\perp}$, and $a=1/\varsigma$, with $\alpha_{f,s}^{\perp}=\beta_{f,s}^{\perp}/(\rho C)_{f,s}$ are, respectively, the normal components of the thermal diffusivities of the Al transducer and the active subjacent semiconductor layer.

The boundary conditions become

$$\frac{\partial\theta_f}{\partial z}(z=0,p)=0,$$

$$\theta_s(\infty,p)=0,$$

$$[\theta_f(z=d_f,p)-\theta_s(z=0,p)]=-R_K\beta_s^{\perp}\frac{\partial\theta_s}{\partial z}(z=0,p), \tag{6}$$

$$\beta_f^{\perp}\frac{\partial\theta_f}{\partial z}(z=d_f,p)=\beta_s^{\perp}\frac{\partial\theta_s}{\partial z}(z=0,p).$$

The solution of the new equation system (5) with the boundary conditions (6) allows us to get the expression of the temperature distribution inside the Al transducer,

$$\theta_f(z,p)=Le^{-q_fz}+Me^{q_fz}+Ne^{-az}. \tag{7}$$

The coefficients L, M, and N are respectively given by

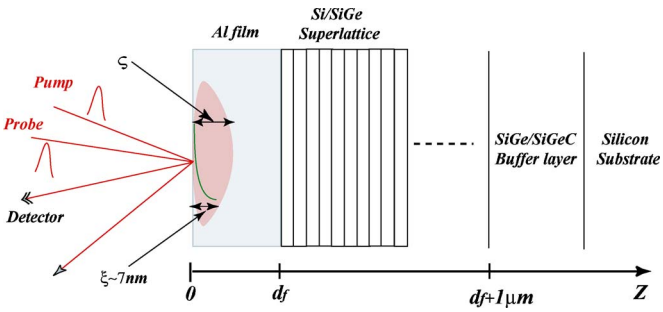

FIG. 2. (Color online) Schematic diagram of the studied structure with a coordinate axis in the cross-plan direction of both Al transducer free surface and $Si/Si_{0.7}Ge_{0.3}$ SL layers.

$$L=\frac{aN}{2q_f}\times\frac{e^{-ad_f}(\Upsilon-q_f/a)-e^{q_fd_f}(1+\Upsilon)}{ch(q_fd_f)+\Upsilon sh(q_fd_f)},$$

$$M=\frac{aN}{2q_f}\times\frac{e^{-ad_f}(\Upsilon-q_f/a)+e^{-q_fd_f}(1-\Upsilon)}{ch(q_fd_f)+\Upsilon sh(q_fd_f)}, \tag{8}$$

$$N=\frac{\chi}{q_f^2-a^2},$$

where the term Υ has the expression $\Upsilon=\beta_f^{\perp}q_f/\beta_s^{\perp}q_s+(d_f/\mathrm{Bi})q_f$. Bi is a defined Biot number with respect to the transducer thickness $\mathrm{Bi}=d_f/R_K\beta_f^{\perp}$.

In a PPTT experience, however, the quantity measured is the reflectivity change rather than the temperature variation, and one has to relate both quantities, which constitutes the next step in the model. This can be achieved by weighting the temperature variation through the optical sensitivity function and integrating it over the metal transducer thickness,[26]

$$\Delta R(t)=\int_0^{d_f}\Delta T_f(z,t)f(z)dz. \tag{9}$$

The optical sensitivity function determines how temperature variations at different depth values below the free surface contribute to the reflectivity change. The general form of $f(z)$ is an exponentially damped oscillation with nonzero phase at the free surface $z=0$. The periodicity of $f(z)$ is half the wavelength of light in the material. The range of $f(z)$ is determined by the optical penetration length ξ as it was calculated by Thomsen *et al.*[26] and Zhu *et al.*[27] In metals, the absorption length is generally much shorter than the wavelength of the laser source (780 nm), and an exponentially decreasing form is a good approximation for $f(z)$,[28]

$$f(z)=f_0\exp\left(-\frac{z}{\xi}\right). \tag{10}$$

This expression fits particularly well in metals which exhibit a large value of the real part of the refraction index. f_0 is a constant which takes into account the energetic profile of the probe and the optical properties of the metal transducer.

In Laplace domain, the combination of formulas (7), (9), and (10) allows us to get the reflectivity change expression,

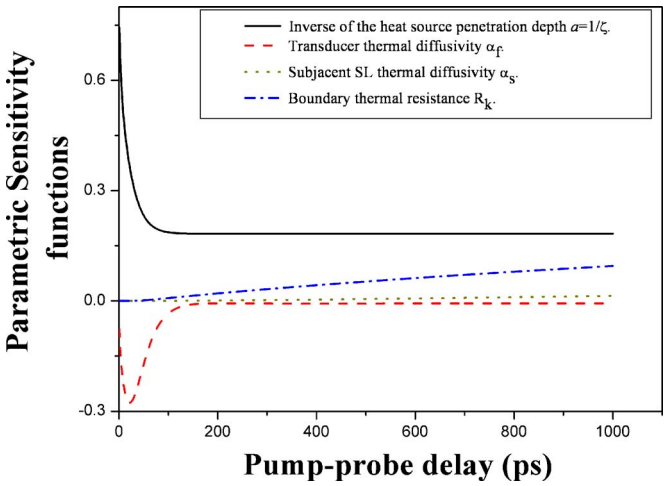

FIG. 3. (Color online) Behavior of the parametric sensitivity functions with respect to different free parameters of the model, as a function of the pump-probe delay.

$$\widetilde{\Delta R}(p) = \int_0^{d_f} \theta_f(z,p) f(z) dz$$
$$= f_0 \left\{ \frac{L}{b+q_f}[1-e^{-(b+q_f)d_f}] + \frac{M}{b-q_f}[1-e^{-(b-q_f)d_f}] + \frac{N}{b+a}[1-e^{-(b+a)d_f}] \right\}, \quad (11)$$

where $b=1/\xi$. A Gaver-Stehfest numerical algorithm allows then to calculate the Laplace inverse transform $\Delta R(t)$.[29]

In expression (11), we have four free parameters which represent the heat source penetration depth ς, the normal components of the thermal diffusivities of the Al transducer and of the subjacent SL layer $\alpha_f^{\perp}$ and $\alpha_s^{\perp}$, respectively, and the thermal boundary resistance R_K at the interface Al transducer/subjacent SL layer. We assume that the optical penetration depth ξ is known at the wavelength of the experiment ($\xi \approx 7$ nm at $\lambda = 780$ nm). A sensitivity study in relation to these four parameters is reported in Fig. 3 as a function of the pump-probe delay. For each parameter X, the parametric sensitivity function is defined by calculating the logarithmic derivative of $\Delta R(t)$ with respect to the logarithm of X,

$$\mathrm{Sens}_X[\Delta R(X,t)] = \frac{\partial \ln[\Delta R(X,t)]}{\partial \ln(X)} = \frac{X}{\Delta R}\frac{\partial \Delta R(X,t)}{\partial X}. \quad (12)$$

The general behavior of these functions as a function of the thermophysical properties of the whole structure (transducer+SL) is rather complex. However, we can see that all parameters are temporally uncorrelated, which means that they can be separately identified. Furthermore, we can notice that the sensitivity of the reflectivity change with respect to the normal component of the thermal diffusivity of the subjacent SL layer $\alpha_s^{\perp}$ is noticeably very weak during the time scale of the experiment.

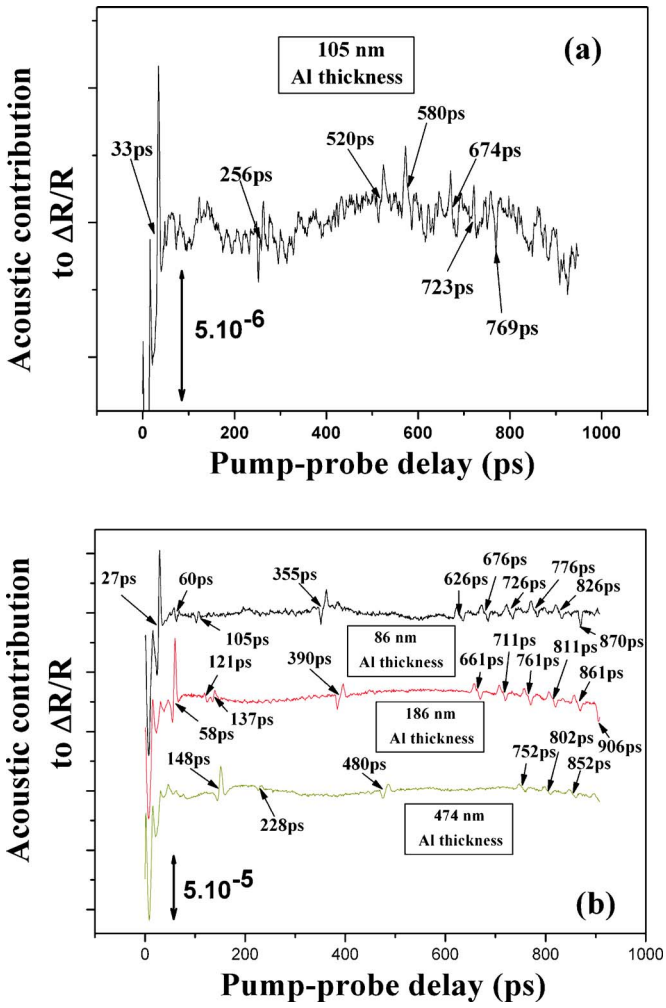

FIG. 4. (Color online) Acoustic contribution to the PPTT signal for the four studied samples after subtraction of the thermal background (a) for 105 nm Al transducer and (b) for 86, 186, and 474 nm Al transducers.

IV. EXPERIMENTAL RESULTS AND DISCUSSION

In this section, we will distinguish between thermal and acoustic contributions to the PPTT signal. Let us begin with the acoustic contribution.

A. Acoustic contribution

Experimental curves show a thermal decay upon which some spikes are superimposed. These spikes arise from acoustic echoes bouncing back and forth inside the structure. Like thermal diffusion, the propagation of the elastic strain inside a layer alters the optical properties of this layer, in particular, those of the transducer; as a consequence, these changes appear in the measured reflectivity signal when the elastic strain reaches the free surface and generates an echo. Acoustic contributions relative to the four samples studied are reported in Fig. 4 after subtraction of the thermal background from curves of Fig. 5. We note here that the thermal background was subtracted after it was fitted with an exponential decay. We distinguish two cases, one without and one with a cap layer between the Al transducer and the active SL layer.

1. Without cap layer

It is the case of the first sample with 105 nm Al transducer. We should note, here, that for this sample, the pump and the probe pulses have, respectively, energies ~1.4 and ~0.2 nJ. The first result we can obtain from the acoustic contribution analysis is the Al transducer thickness at the point impact of both the pump and the probe beams. The thickness is deduced from the measurement of the flight time of the first acoustic echo and the knowledge of the normal component of the sound velocity inside the Al film,

$$d_{\mathrm{Al}} = \frac{v_{\mathrm{Al}} \times t_{1\mathrm{st\ echo}}}{2}. \tag{13}$$

Usually, Young's modulus of aluminium films which are deposited with electron beam evaporation does not vary strongly as a function of the deposition conditions. Young's modulus (~70 GPa) and also the sound velocity (~6400 m/s) are the same as those of bulk materials.[30] We find a thickness of 105 nm with incertitude of 3 nm. This incertitude about the transducer thickness is due to the temporal resolution of our experimental setup which is 1 ps.

In the approximation of an effective optical and acoustical medium, density ρ_{SL}, heat capacity per unit volume C_{SL}, and the normal component of the sound velocity v_{SL} of the $Si/Si_{0.7}Ge_{0.3}$ SL are given respectively by[31]

$$\begin{aligned} &\rho_{\mathrm{SL}} d_b = \rho_1 d_1 + \rho_2 d_2, \\ &C_{\mathrm{SL}} d_b = C_1 d_1 + C_2 d_2, \\ &\frac{d_b}{\rho_{\mathrm{SL}} v_{\mathrm{SL}}^2} = \frac{d_1}{\rho_1 v_1^2} + \frac{d_2}{\rho_2 v_2^2}, \\ &d_b = d_1 + d_2. \end{aligned} \tag{14}$$

$\rho_{i,j}$, $C_{i,j}$, $v_{i,j}$, and $d_{i,j}$ are, respectively, density, heat capacity per unit volume, normal component of the sound velocity, and thickness of the layer i, j.

Figure 4(a) reports the acoustic contribution of the first sample with 105 nm Al film. In addition to the first acoustic echo, we can see a second echo and an acoustic burst of five successive echoes. The measurement of the flight time difference between both first and second echoes in conjunction with the knowledge of the $Si/Si_{0.7}Ge_{0.3}$ SL thickness allows us to deduce the value of the normal component of the sound velocity inside the SL,

$$v_{\mathrm{SL}} = \frac{2 d_{\mathrm{SL}}}{t_{2\mathrm{nd\ echo}} - t_{1\mathrm{st\ echo}}}. \tag{15}$$

For this sample, we find a value of $v_{\mathrm{SL}}^{\mathrm{exp}} \simeq (8.93 \pm 0.33)$ nm/ps, which is about 13% higher than the estimated value from formula (14) which leads to $v_{\mathrm{SL}}^{\mathrm{theo}} \simeq 7.79$ nm/ps.

2. With cap layer

Figure 4(b) shows the acoustic contributions relative to the three other samples. For these samples, the pump and the probe pulses energies were, respectively, ~1, and ~0.1 nJ.

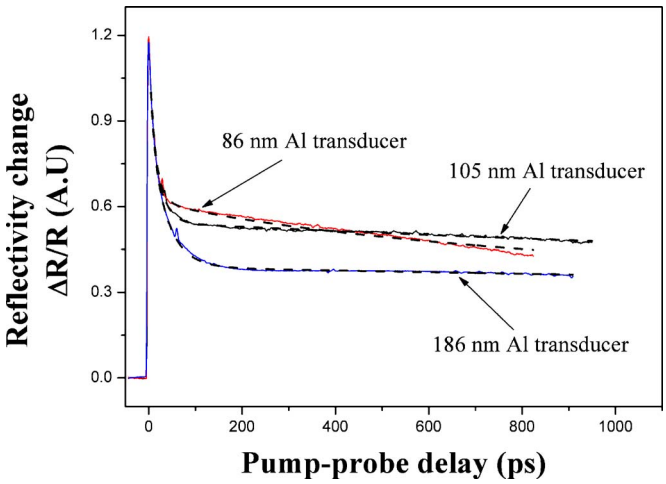

FIG. 5. (Color online) Comparison between experimental PPTT signals (solid lines) and theoretical curves (dashed lines) for three Al transducer thicknesses, all curves are normalized with respect to the value at 5 ps. For 105 nm Al transducer, the pump and the probe pulses have energies ~1.4 and ~0.2 nJ, respectively. On the other hand, for 86 and 186 nm Al transducers, the pump and the probe pulses energies were, respectively, ~1, and ~0.1 nJ. The absolute change in the relative reflectivity depends on the pump power; in our case, it was within the range of 10^{-4}–6×10^{-3}.

By contrast to the first case, the analysis of the first echoes flight time differences is incompatible with the knowledge of the SL thickness, but suggests the presence of an additive layer, which is a $Si_{0.9}Ge_{0.1}$ cap layer, between the Al transducer and the $Si/Si_{0.7}Ge_{0.3}$ SL. From an acoustic stance, the presence of a cap layer does not prevent the characterization of acoustic properties of the SL and of the buffer layer. In this case also, using formula (13) allows us to obtain the thickness of the Al transducer, we find, respectively, 86, 186, and 474 nm. As can be seen in Fig. 4(b), for 86 and 186 nm Al transducers, the phase inversion between the first and the second echoes lets us think about a second reflection on the same interface; the second echo comes from the same interface Al transducer/cap layer. This second reflection disappears in the case of 474 nm Al transducer because of the acoustic attenuation within the thick metal film.[32,33] Indeed, we can see that the first acoustic echo amplitude decreases as the thickness of the Al transducer increases; the acoustic attenuation then affects all the following echoes.

The measurement of the flight time difference between the first and the third echoes in the case of 86 and 186 nm Al transducers, and between the first and the second echoes in the case of 474 nm Al transducer, in conjunction with the estimation of the normal component of the sound velocity inside the cap layer, allows us to deduce the cap thickness using a formula similar to (13).

Similarly, from the flight time difference measurement between the third and the fourth echoes for both 86 and 186 nm Al transducer samples, and between the second and the third echoes for 474 nm Al transducer sample, in conjunction with the knowledge of the SL thickness, we can extract the value of the normal component of the sound velocity within the SL layer using a similar formula of (15). This value is then compared to the estimated value from formula (14).

TABLE I. Identified acoustic properties from acoustic contribution analysis of the PPTT signal of the four studied samples.

Properties	Sample 1 (105 nm Al transducer)	Sample 2 (86 nm Al transducer)	Sample 3 (186 nm Al transducer)	Sample 4 (474 nm Al transducer)
Cap layer	No	Yes	Yes	Yes
1st echo (ps)	33	27	58	148
d_f (nm)	105	86	186	474
v_{cap} (nm/ps)[a]	···	7.79	7.79	7.79
d_{cap} (nm)	···	304	308	312
d_{SL} (nm)[b]	996	996	996	996
v_{SL} (nm/ps)	8.93	7.97	7.87	7.9
d_{buf} (nm)[b]	1000	1000	1000	1000
v_{buf} (nm/ps)	7.57	7.38	7.38	7.35

[a]Estimated theoretical value from formula (14).
[b]Given values from growth process.

Added to these results, for each sample studied, at $t > 500$ ps, we can observe an acoustic burst of exactly five echoes separated by the same temporal interval of 50 ps. This sequence of acoustic echoes is the signature of the presence of five buried layers within the buffer layer as shown in Fig. 1(b). Table I lists all acoustic properties deduced from the acoustic contributions analysis of the four samples studied. As we can see in this table, the value of the normal component of the sound velocity of the $Si/Si_{0.7}Ge_{0.3}$ SL for samples of Fig. 4(b) is very close to the theoretical estimated value, the difference being less than 3%.

B. Thermal contribution

The analysis of the thermal contribution to the PPTT signal consists in comparing theoretical curves to experimental results obtained from three of the four samples studied. Both experimental and theoretical curves are normalized with respect to the value at 5 ps, point of time from when we can consider the diffusive regime with one macroscopic temperature to be established as shown in Sec. III.

In the case of thick Al transducer (474 nm), because of the short time scale of the experiment, heat does not have enough time to cross the transducer completely. The theoretical model we have developed cannot capture the behavior of heat diffusion in this particular case; this is why the experimental result corresponding to this Al transducer thickness is not compared with the theoretical model, and only analysis of the acoustic contribution to the PPTT signal is being considered.

Figure 5 shows a comparison between experimental and theoretical curves for 86, 105, and 186 nm Al transducers. Theoretical curves were obtained by optimizing free parameters (ς, R_K, $\alpha_f^{\perp}$, and $\alpha_s^{\perp}$). The absolute change in the relative reflectivity depends on the pump power; in our case, it was within the range of $10^{-4}-6\times10^{-3}$. For all samples, there is a fast thermal decay characteristic of heat diffusion inside the Al film, followed by a slow decay, characteristic of heat diffusion inside the subjacent SL or cap layers.

The experimental curves can be divided into two parts, the first part with a fast thermal decay depends mainly on the transducer properties, which are the heat source penetration depth ς and the normal component of the thermal diffusivity $\alpha_f^{\perp}$. The second part is controlled by the subjacent semiconductor layer properties, especially the boundary thermal resistance R_K. This is confirmed by the parametric sensitivity study. As shown in Fig. 3, during the time scale of the experiment (~1 ns), $\Delta R(t)$ is more sensitive to R_K than to $\alpha_s^{\perp}$.

TABLE II. Identified thermal properties from thermal contribution analysis of the PPTT signal of three of the four studied samples.

Properties	Sample 1 (105 nm Al transducer)	Sample 2 (86 nm Al transducer)	Sample 3 (186 nm Al transducer)
Cap layer	No	Yes	Yes
Heat source penetration depth ς (nm)	37.5	34	44
Thermal boundary resistance at the interface Al transducer/subjacent layer (m^2 K/W)	2.2×10^{-8}	5.3×10^{-9}	1.8×10^{-8}
Normal component of the thermal diffusivity of the Al transducer (m^2/s) (Bulk value 9.7×10^{-5} m^2/s)	5.86×10^{-5}	5.86×10^{-5}	9.7×10^{-5}

In the case of 105 nm Al transducer (sample without cap layer), we used the extracted value of $\alpha_s^{\perp}$ for the $Si/Si_{0.7}Ge_{0.3}$ SL; this value was identified in a previous study where the SL was covered by a very thin Al film.[34]

Thermally, for samples with 86 and 186 nm Al transducers (samples with cap layer), the presence of the cap layer hides completely the SL, and all identified thermophysical properties correspond to this layer. In fact, at the time scale of the experiment (~1 ns), heat has not enough time to reach the SL, and penetrates only some tenths of nanometer within the cap layer. In this case, we used as value of the normal component of the thermal diffusivity $\alpha_s^{\perp}$ the identified value by Huxtable *et al.*[10]

Optimization of the free parameters for the three samples gives the values recapitulated in Table II. As we can see, for all samples, the heat source penetration depth ς largely exceeds the optical penetration depth ξ. This difference proves that with a thick metal transducer, it is necessary to distinguish between both parameters in a PPTT for a good interpretation and exploitation of experimental results.[35] Although identified values of boundary resistance are not the same for the three samples, they are of the same order of magnitude as the reported values in the literature[36–38], and the fact that this parameter is closely related to the metal transducer thickness is noteworthy; a small change of the transducer thickness produces a significant change in the value of the optimized R_K; the error can easily reach 30% and more. The boundary thermal resistance (Kapitza resistance) depends on several parameters which we can resume as (i) the interface quality, (ii) the difference of acoustic properties of both materials constituting the interface, (iii) Debye temperature difference of both materials, (iv) the nature of heat transfer across the interface, in such a way that the process includes only phonons, or phonons and electrons, (v) the carriers scattering nature on the interface, elastic or inelastic, and finally (vi) the anharmonicity of the lattice po-

tential on both sides of the interface.[37] For the 186 nm Al film, bulk value for the thermal diffusivity $\alpha_f^{\perp}$ has allowed to get a good fit of the experimental curve, as opposed to Al transducer with lesser thickness, for which $\alpha_f^{\perp}$ value is lower.

In this section, we have not discussed acoustic echoes forms. However, we should note that in our case with the used values of $\alpha_f^{\perp}$, heat diffuses along optical penetration depth faster than sound, and then heat diffusion within the Al transducer affects the formation of acoustic field. We focused instead on acoustic echoes, flight times, and their use to extract either the thickness, or the normal component of the sound velocity, of the different layers forming the samples studied.

V. CONCLUSION

A pump-probe thermoreflectance technique (PPTT) is used for the characterization of phonon transport in the cross plan direction of $Si/Si_{0.7}Ge_{0.3}$ superlattice samples at room temperature. Both thermal and acoustic contributions to the PPTT signal are analyzed and thermal and acoustic properties of both metal transducer and subjacent SL or cap layer are identified. The results are in good agreement with reported data in the literature. The effects of the transducer thickness, the electron diffusion, and the pump-probe delay are clearly shown. To be more sensitive to the thermal properties of the underlying active SL, a long pump-probe delay is needed with a thin metal transducer to overcome electron diffusion inside it. Moreover, analysis of acoustic contribution shows the PPTT to be a pertinent echographical technique of submicrometer scale systems.

ACKNOWLEDGMENTS

The authors would like to thank Pr Ali Shakouri and his group for manufacturing and providing samples and for all helpful discussions. This work is supported by "La Région d'Aquitaine," FEDER, and "Le Ministère de la Recherche" (CPER).

[1]P. Y. Yu and M. Cardona, *Fundamentals of Semiconductors: Physics and Materials Properties* (Springer, Berlin, 2001), p. 578.
[2]P. Y. Yu and M. Cardona, *Fundamentals of Semiconductors: Physics and Materials Properties*, 3rd ed. (Springer, Berlin, 2001).
[3]S. M. Sze, *Physics of Semiconductor Devices*, 2nd ed., (Wiley, New York, 1981).
[4]R. Venkatasubramanian, E. Siivola, T. Colpitts, and B. O'Quinn, Nature (London) **413**, 597 (2001).
[5]T. C. Harman, P. J. Taylor, M. P. Walsh, and B. E. Laforge, Science **297**, 2229 (2002).
[6]S. M. Lee, D. G. Cahill, and R. Venkatasubramanian, Appl. Phys. Lett. **70**, 2957 (1997).
[7]W. S. Capinski and H. J. Maris, Physica B **219/220**, 699 (1996).
[8]W. S. Capinski, M. Cardona, D. S. Katzer, H. J. Maris, K. Ploog, and T. Ruf, Physica B **263/264**, 530 (1999).
[9]W. S. Capinski, H. J. Maris, T. Ruf, M. Cardona, K. Ploog, and D. S. Katzer, Phys. Rev. B **59**, 8105 (1999).
[10]S. T. Huxtable *et al.*, Appl. Phys. Lett. **80**, 1737 (2002).
[11]M. N. Touzelbaev, P. Zhou, R. Venkatasubramanian, and K. E. Goodson, J. Appl. Phys. **90**, 763 (2001).
[12]T. Yao, Appl. Phys. Lett. **51**, 1798 (1987).
[13]D. G. Cahill, K. E. Goodson, and A. Majumdar, J. Heat Transfer **124**, 223 (2002).
[14]R. Venkatasubramanian, Phys. Rev. B **61**, 3091 (2000).
[15]G. Chen, Phys. Rev. B **57**, 14958 (1998).
[16]M. V. Simkin and G. D. Mahan, Phys. Rev. Lett. **84**, 927 (2000).
[17]B. Yang and G. Chen, Phys. Rev. B **67**, 195311 (2003).
[18]D. G. Cahill, Rev. Sci. Instrum. **61**, 802 (1990).
[19]C. A. Paddock and G. L. Eesley, J. Appl. Phys. **60**, 285 (1986).
[20]D. G. Cahill, W. K. Ford, K. E. Goodson, G. D. Mahan, A. Majumdar, H. J. Maris, R. Merlin, and S. R. Phillpot, J. Appl. Phys. **93**, 793 (2003).
[21]J. P. Douglas, Int. J. Heat Mass Transfer **19**, 75 (2004).
[22]T. Q. Qiu and C. L. Tien, J. Heat Transfer **35**, 719 (1992).
[23]T. Q. Qiu and C. L. Tien, J. Heat Transfer **115**, 835 (1993).
[24]G. Tas and H. J. Maris, Phys. Rev. B **49**, 15046 (1994).
[25]F. P. Incropera and D. P. Dewitt, *Introduction to Heat Transfer*, 2nd ed. (Wiley, New York, 1990).
[26]C. Thomsen, H. T. Grahn, H. J. Maris, and J. Tauc, Phys. Rev. B **34**, 4129 (1986).
[27]T. C. Zhu, H. J. Maris, and J. Tauc, Phys. Rev. B **44**, 4281 (1991).
[28]B. Bonello, B. Perrin, and C. Rossignol, J. Appl. Phys. **83**, 3081 (1998).
[29]D. Maillet, S. André, J. C. Batsale, A. Degiovanni, and C. Moyne, *Thermal Quadrupoles: Solving the Heat Equation through Integral Transforms* (Wiley, New York, 2000).
[30]D. M. Profunser, J. Vollmann, and J. Duan, Ultrasonics **42**, 641 (2004).
[31]C. Rossignol, B. Perrin, B. Bonello, P. Djemia, P. Moch, and H. Hurdequint, Phys. Rev. B **70**, 094102 (2004).
[32]O. B. Wright, J. Appl. Phys. **71**, 1617 (1992).
[33]H. N. Lin, R. J. Stoner, H. J. Maris, and J. Tauc, J. Appl. Phys. **69**, 3816 (1991).
[34]Y. Ezzahri, S. Dilhaire, S. Grauby, J. M. Rampnoux, W. Claeys, Y. Zhang, G. Zeng, and A. Shakouri, Appl. Phys. Lett. **87**, 103506 (2005).
[35]Y. Ezzahri, S. Grauby, S. Dilhaire, J. M. Rampnoux, W. Claeys, Y. Zhang, and A. Shakouri, 11th International Workshop on Thermal Investigations of ICs and Systems (THERMINICS), 27–30 September 2005, Belgirate, pp. 235–243.
[36]R. J. Stoner, H. J. Maris, T. R. Anthony, and W. F. Banholzer, Phys. Rev. Lett. **68**, 1563 (1992).
[37]R. J. Stoner and H. J. Maris, Phys. Rev. B **48**, 16373 (1993).
[38]A. N. Smith, J. L. Hostetler, and P. M. Norris, Microscale Thermophys. Eng. **4**, 51 (2000).